CORONAVIRUS

SARS-CoV-2 mutations in MHC-I–restricted epitopes evade CD8$^+$ T cell responses

Benedikt Agerer[1†], Maximilian Koblischke[2†], Venugopal Gudipati[3†], Luis Fernando Montaño-Gutierrez[4], Mark Smyth[1], Alexandra Popa[1], Jakob-Wendelin Genger[1], Lukas Endler[1], David M. Florian[2], Vanessa Mühlgrabner[3], Marianne Graninger[2], Stephan W. Aberle[2], Anna-Maria Husa[4], Lisa Ellen Shaw[5], Alexander Lercher[1‡], Pia Gattinger[6], Ricard Torralba-Gombau[1], Doris Trapin[7], Thomas Penz[1], Daniele Barreca[1], Ingrid Fae[8], Sabine Wenda[8], Marianna Traungott[9], Gernot Walder[10], Winfried F. Pickl[7,11], Volker Thiel[12,13], Franz Allerberger[14], Hannes Stockinger[3], Elisabeth Puchhammer-Stöckl[2], Wolfgang Weninger[5], Gottfried Fischer[7], Wolfgang Hoepler[9], Erich Pawelka[8], Alexander Zoufaly[8], Rudolf Valenta[3,6,11,15,16], Christoph Bock[1,17], Wolfgang Paster[4], René Geyeregger[4], Matthias Farlik[5], Florian Halbritter[4], Johannes B. Huppa[3†], Judith H. Aberle[2†], Andreas Bergthaler[1*†]

CD8$^+$ T cell immunity to SARS-CoV-2 has been implicated in COVID-19 severity and virus control. Here, we identified nonsynonymous mutations in MHC-I–restricted CD8$^+$ T cell epitopes after deep sequencing of 747 SARS-CoV-2 virus isolates. Mutant peptides exhibited diminished or abrogated MHC-I binding in a cell-free in vitro assay. Reduced MHC-I binding of mutant peptides was associated with decreased proliferation, IFN-γ production, and cytotoxic activity of CD8$^+$ T cells isolated from HLA-matched patients with COVID-19. Single-cell RNA sequencing of ex vivo expanded, tetramer-sorted CD8$^+$ T cells from patients with COVID-19 further revealed qualitative differences in the transcriptional response to mutant peptides. Our findings highlight the capacity of SARS-CoV-2 to subvert CD8$^+$ T cell surveillance through point mutations in MHC-I–restricted viral epitopes.

INTRODUCTION

SARS-CoV-2 infection elicits broad activation of the innate and adaptive arms of immunity (*1*–*4*). Major correlates of protection are neutralizing antibodies and cytotoxic CD8$^+$ T lymphocytes (CTLs) (*5*). CTLs play an essential role in conferring immune memory and protection against viral pathogens (*6*–*8*). CTLs kill infected cells upon recognition of viral epitopes because they are displayed on the cell surface in the context of the class I major histocompatibility complex proteins (MHC-I). Certain positions in these epitopes have been shown to be critical for MHC-I presentation, and mutations in these so-called anchor residues might interfere with peptide binding to MHC-I (*9*, *10*). CTL responses have been described in great detail in SARS-CoV-2–infected patients (*3*, *4*, *11*–*15*). In acute SARS-CoV-2 infection, CTLs show high levels of cytotoxic effector molecules, such as granzyme B, perforin, and interferon-γ (IFN-γ) (*16*). Numerous human leukocyte antigen (HLA)–restricted CTL epitopes have been characterized for SARS-CoV-2 (*4*, *14*, *17*–*21*).

Compelling evolutionary evidence for CTL-mediated control of RNA viruses causing chronic infections, such as HIV and hepatitis C virus (HCV), is provided by mutations occurring in viral epitopes, which directly interfere with MHC-I–restricted T cell antigen recognition and killing by CTLs (*22*–*25*). Although several mutations in SARS-CoV-2 have recently been associated with an escape from antibody responses (*26*–*28*), the extent to which SARS-CoV-2 mutations may upend the presentation of virus-derived peptides via MHC-I remains to be determined. In this study, we used deep viral genome sequencing to identify nonsynonymous mutations in previously reported MHC-I epitopes. We applied a combination of cell-free in vitro assays, as well as functional and transcriptional characterization of COVID-19 patient–derived peripheral blood mononuclear cells (PBMCs) to investigate the potential of single point mutations in MHC-I epitopes to evade CTL responses.

RESULTS

Bioinformatic analysis of mutations in putative SARS-CoV-2 CD8$^+$ T cell epitopes

To assess a possible impact of virus mutations on SARS-CoV-2–specific CD8$^+$ T cell responses, we performed deep viral genome sequencing (>20,000× coverage) (fig. S1A) and bioinformatic analysis on 747 SARS-CoV-2 samples (*14*). We focused on 27 CTL epitopes, which had previously been reported as experimentally validated

[1]CeMM Research Center for Molecular Medicine of the Austrian Academy of Sciences, Vienna, Austria. [2]Center for Virology, Medical University of Vienna, Vienna, Austria. [3]Institute for Hygiene and Applied Immunology, Center for Pathophysiology, Infectiology and Immunology, Medical University of Vienna, Vienna, Austria. [4]St. Anna Children's Cancer Research Institute (CCRI), Vienna, Austria. [5]Department of Dermatology, Medical University of Vienna, Vienna, Austria. [6]Department of Pathophysiology and Allergy Research, Division of Immunopathology, Medical University of Vienna, Vienna, Austria. [7]Institute of Immunology, Center for Pathophysiology, Infectiology and Immunology, Medical University of Vienna, Vienna, Austria. [8]Department of Blood Group Serology and Transfusion Medicine, Medical University of Vienna, Vienna, Austria. [9]Department of Medicine 4, Clinic Favoriten, Vienna, Austria. [10]Division of Hygiene and Medical Microbiology, Medical University of Innsbruck, Innsbruck, Austria. [11]Karl Landsteiner University of Health Sciences, Krems, Austria. [12]Institute of Virology and Immunology, Bern and Mittelhäusern, Switzerland. [13]Department of Infectious Diseases and Pathobiology, Vetsuisse Faculty, University of Bern, Bern, Switzerland. [14]Austrian Agency for Health and Food Safety (AGES), Vienna, Austria. [15]Laboratory for Immunopathology, Department of Clinical Immunology and Allergy, First Moscow State Medical University Sechenov, Moscow, Russia. [16]NRC Institute of Immunology FMBA of Russia, Moscow, Russia. [17]Department of Laboratory Medicine, Medical University of Vienna, Vienna, Austria.
*Corresponding author. Email: abergthaler@cemm.oeaw.ac.at
†These authors contributed equally to this work.
‡Present address: Laboratory of Virology and Infectious Disease, Rockefeller University, New York, NY, USA.

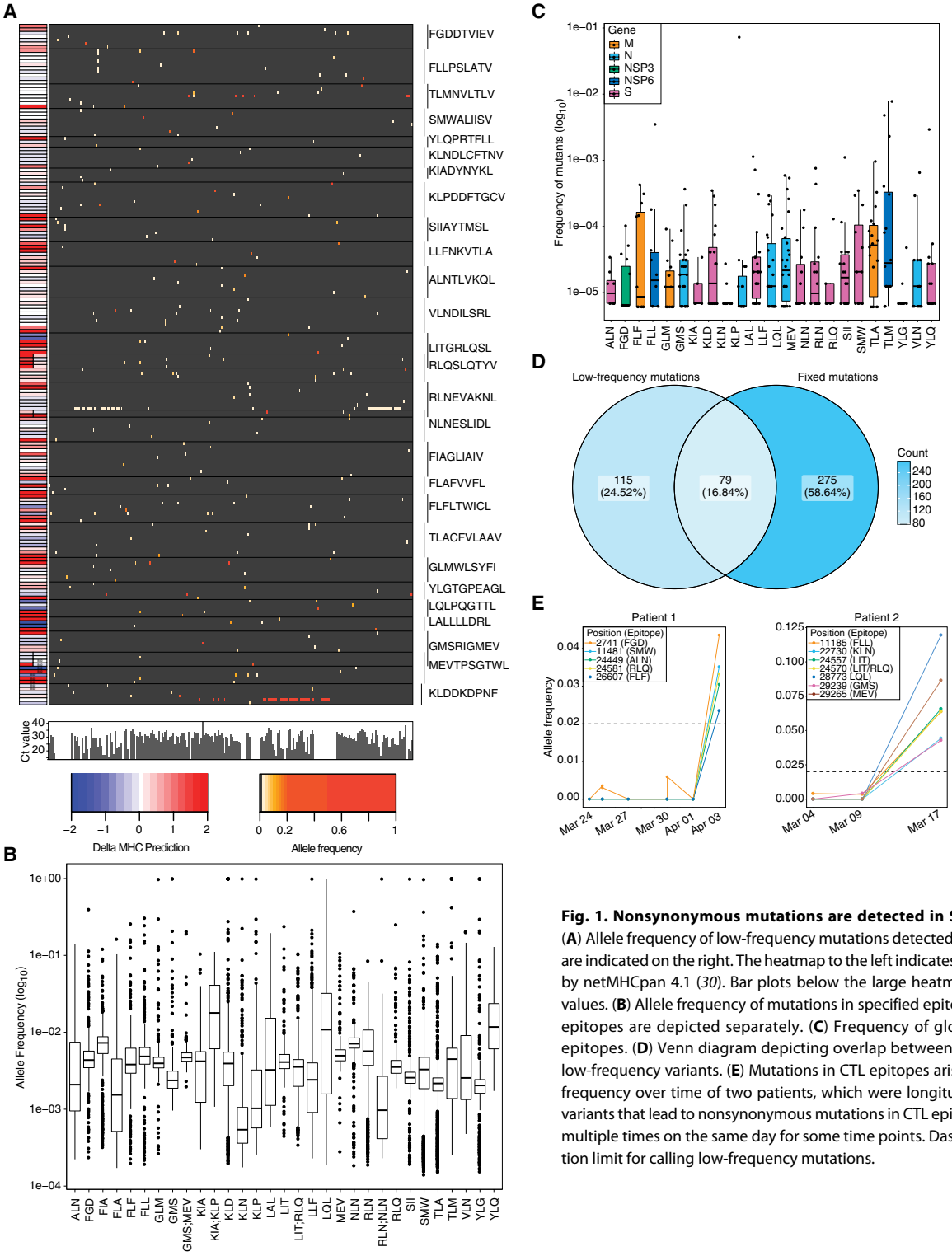

Fig. 1. Nonsynonymous mutations are detected in SARS-CoV-2 CTL epitopes. (**A**) Allele frequency of low-frequency mutations detected in 27 CTL epitopes. Epitopes are indicated on the right. The heatmap to the left indicates change in % ranks predicted by netMHCpan 4.1 (*30*). Bar plots below the large heatmap indicate viral loads as Ct values. (**B**) Allele frequency of mutations in specified epitopes. Regions present in two epitopes are depicted separately. (**C**) Frequency of global fixed mutations in CTL epitopes. (**D**) Venn diagram depicting overlap between global fixed mutations and low-frequency variants. (**E**) Mutations in CTL epitopes arise late in infection. Mutation frequency over time of two patients, which were longitudinally sampled. Shown are variants that lead to nonsynonymous mutations in CTL epitopes. Patient 1 was sampled multiple times on the same day for some time points. Dashed lines indicate the detection limit for calling low-frequency mutations.

epitopes restricted by HLA-A*02:01 (allele frequency 0.29 in Austria) or HLA-B*40:01 (allele frequency 0.03 to 0.05 in Austria) (*4*, *17*–*20*, *29*). Most of the selected epitopes are located in the S protein ($N = 13$), and the remaining epitopes are distributed between the N ($N = 6$), ORF1ab ($N = 4$), M ($N = 3$), and E ($N = 1$) proteins. Detailed descriptions of peptides and their three-letter codes are listed in table S1. Among these epitopes, we detected 194 nonsynonymous mutations present at frequencies of ≥0.02 in 229 samples (Fig. 1, A and B). Of these 194 variants, 35 were found at frequencies between 0.1 and 0.5. Nine variants were fixed

(frequency ≥ 0.9) and found in 53 different patient samples (table S2). Because of overlaps in some epitopes, these 194 mutations result in 199 different epitope variants. Forty-one of these mutations were localized to anchor residues, and 21 mutations affected auxiliary residues, which are both integral to MHC-I peptide loading (fig. S1B) (*9*, *10*). Prediction of the binding strength of the wild-type (WT) and mutant peptides to HLA-A*02:01 and HLA-B*40:01 via NetMHCpan v4.1 (*30*) revealed weaker peptide binding to MHC-I, as indicated by an increase of NetMHCpan % ranks (fig. S1, C to F). For many of the investigated CTL epitopes, we detected multiple variants that independently emerged in different SARS-CoV-2–infected individuals (Fig. 1A). To corroborate these findings from low-frequency mutations in our deep sequencing dataset, we analyzed fixed mutations in >145,000 available global SARS-CoV-2 sequences from the public database Global Initiative on Sharing All Influenza Data (GISAID) (*31*). Mutations were observed in 0.0000689 to 7.336% epitope sequences (mean = 0.005106%) (Fig. 1C). We found 10 to 11,717 viral genome sequences with a nonsynonymous mutation for each of the investigated 27 CTL epitopes (mean = 807.05). We found fixed variants in GISAID that were also identified in our low-frequency analysis, highlighting the relevance of individual low-frequency mutations (Fig. 1D and fig. S1, G and H).

To examine the time dynamics of low-frequency epitope mutations in patients, we used serially sampled viral genomes from patients with COVID-19. Suggestive of CTL-mediated selection pressures, mutations in viral epitopes arose typically later in infection (Fig. 1E). On the basis of our analysis of low-frequency and fixed mutations, we selected 11 WT and 17 corresponding mutant peptides with predicted decreased HLA-binding strength for further biophysical and functional analyses (table S3).

Mutations in CTL epitopes destabilize MHC-I complexes

To assess the MHC-I–dependent immunogenic properties of nonsynonymous mutant peptides, we produced MHC-I complexes with ultraviolet light cleavable peptides (UVCP) and performed peptide exchange reactions to destabilize and later reassemble MHC-I UVCP complexes (*32*). We next used cell-free differential scanning fluorimetry (DSF) to measure the thermal stability of destabilized or reassembled MHC-I complexes (Fig. 2, A to E, and fig. S2, A to L) (*33*–*35*). As shown in fig. S1 (A and B), HLA-A*02:01-UVCP complex is destabilized upon exposure to UV light and can be reassembled by adding UVCP peptide after UV exposure. The minima of the curves specify the melting temperature (T_m) of the HLA-peptide complexes. T_m values well above 37°C indicate strong peptide binding to MHC-I at

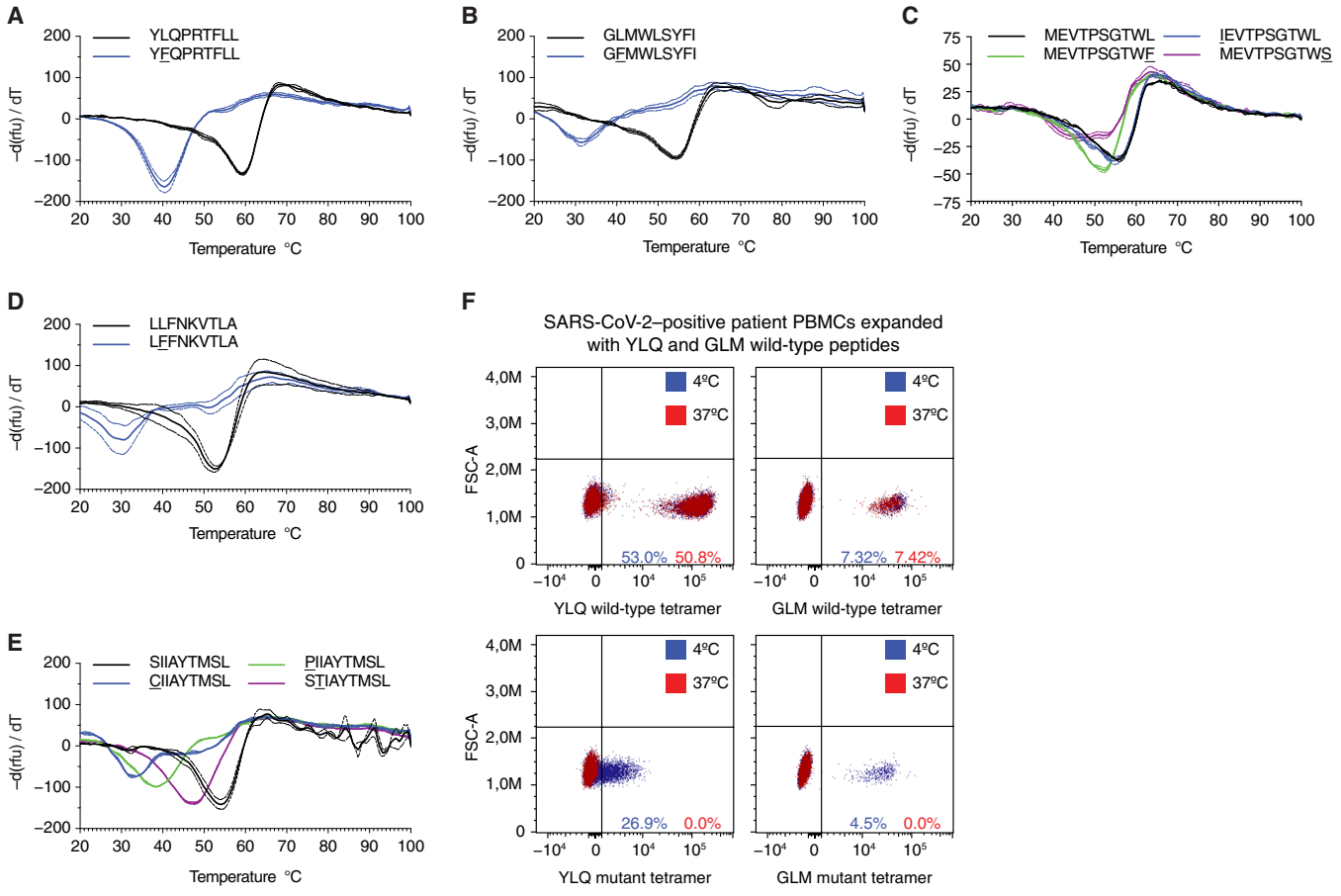

Fig. 2. Epitope variants lead to diminished MHC-I binding. (**A** to **E**) Decreased thermostability of mutant peptide MHC-I complexes. Negative first derivative of rfu plotted against increasing temperatures. Curves for WT peptides are black; mutated peptides are colored. The minimum point of the curves represents the T_m of peptide–MHC-I complexes. Dashed lines indicate SD. $n = 2$ to 3 technical replicates. (**F**) Tetramers featuring mutated peptides are unstable at 37°C. FACS plots showing staining of in vitro expanded PBMCs stained with tetramers containing WT (top) or mutant (bottom) peptides incubated at 4°C (blue) or 37°C (red).

physiological temperatures, whereas values around 37°C correlate only with weak and below 36°C with absent binding. For 9 of the 11 WT peptides, we observed binding to HLA-A*02:01 or HLA-B*40:01, indicating that these peptides can in principle be presented by the respective HLA allele (fig. S2, C and D). In contrast, 11 analyzed mutants exhibited decreased stabilizing capacity toward MHC-I (Fig. 2, A to E; fig. S2, D and F to L; and table S4). The HLA-B*40:01–restricted MEVTPSGTWL peptide featured specific binding to recombinant HLA-B*40:01 but not to HLA-A*02:01 (Fig. 2C and fig. S2L) (*4*). An example of a weak binder is the mutant variant YFQPRTFLL (instead of YLQPRTFLL), whereas LFFNKVTLA (instead of LLFNKVTLA) represents a nonbinder for HLA-A*02:01 (Fig. 2, A to D). We did neither observe binding of the WT nor the mutant peptides to HLA-A*02:01 for the published CTL epitopes LQLPQGTTL and LALLLLDRL (fig. S2, I and L).

To further corroborate these results, we generated peptide-loaded HLA-A*02:01 and HLA-B*40:01 tetramers presenting WT and mutant peptides as a means to identify cognate $CD8^+$ T cells from expanded PBMCs of HLA-matched COVID-19 patients. As shown in Fig. 2F, tetramers loaded with mutant peptides stain cognate T cells in a T cell receptor (TCR)–dependent fashion when kept at 4°C. However, when tetramers were incubated at 37°C before their use, T cell staining was abrogated most likely because of peptide loss and structural disintegration of MHC-I. Together, these results imply that mutations found in SARS-CoV-2 genome sequences decrease peptide–MHC-I stability and subsequently could promote immune evasion from HLA-dependent recognition by CTLs.

Investigation of epitope responses in SARS-CoV-2–positive patient PBMCs

Next, we investigated peptide-specific $CD8^+$ T cell responses in PBMCs isolated from HLA-A*02:01– or HLA-B*40:01–positive COVID-19 patients (Fig. 3A and tables S5 and S6). We first screened the nine WT peptides, which showed MHC-I binding in the DSF assay, using ex vivo enzyme-linked immune absorbent spot (ELISpot) assays (table S7). None of the five prepandemic healthy controls gave responses to any of the peptides. Further, we could detect a positive response in at least one patient for four of the peptides, which were investigated in additional assays. To this end, HLA-matched PBMCs from patients with COVID-19 and five prepandemic controls were stimulated with peptides and cultured for 10 to 12 days followed by tetramer staining (Fig. 3B). This allowed us to confirm these WT peptides as bona fide T cell epitopes in SARS-CoV-2. We further corroborated virus-specific CTL responses by intracellular cytokine staining (ICS) for IFN-γ after peptide-mediated restimulation (fig. S3, A and B). To investigate the extent to which identified mutations in viral epitopes affected T cell proliferation, we stained WT or mutant peptide–expanded PBMCs with WT peptide–loaded HLA tetramers. We found fewer tetramer-positive $CD8^+$ T cells in PBMCs expanded in the presence of mutant peptides, indicating that mutant peptides featured significantly reduced immunogenicity (Fig. 3, C to F). Consistent with this, ICS for IFN-γ revealed significantly diminished CTL responses after restimulation with mutant peptide as compared with the corresponding WT peptides (Fig. 3, G to J). We observed markedly diminished CTL responses to several mutant peptides both presented in the context of HLA-A*02:01 and HLA-B*40:01. This was further supported by peptide titration experiments involving WT peptides and their mutant counterparts for T cell stimulation (fig. S3C). To complement intracellular cytokine measurements, we also carried out ex vivo ELISpot assays after stimulating PBMCs with WT or mutant peptides without extended expansion. These experiments confirmed that stimulation with mutant peptides resulted in significantly fewer cytokine-producing cells than with WT peptides (Fig. 3K and fig. S3D). To further corroborate these results, we performed functional cytotoxicity assays with PBMCs isolated from four patients with COVID-19, expanded for 10 to 12 days in the presence of WT or mutant YLQPRTFLL (YLQ) peptide. We assessed the ability of these cells to kill autologous Epstein-Barr virus (EBV)–transformed lymphoblastoid B cell lines (EBV^+ B cells) that were pulsed with either WT or mutant YLQ. Although WT-expanded PBMCs showed specific killing of WT-pulsed EBV^+ cells, they failed to kill EBV^+ B cells pulsed with mutant peptide (Fig. 3L), suggesting that mutant YLQ is not properly presented by the EBV^+ B cells. Furthermore, PBMCs expanded with mutant peptides failed to kill both WT and mutant peptide–pulsed EBV^+ B cells (Fig. 3L and fig. S3E). These results further underline that expansion with the mutant peptide failed to mount a functional CTL response.

Transcriptional single T cell analysis upon stimulation with WT or mutant peptides

To further characterize our results from patient PBMCs, we expanded PBMCs isolated from two patients (SARS042 and SARS060) for 10 to 12 days in the presence of WT or mutant YLQ peptide. We sorted equal numbers of YLQ tetramer-positive and tetramer-negative $CD8^+$ T cells for each condition, labeled them with oligonucleotide-barcoded antibodies (TotalSeq anti-human Hashtag), and performed single-cell RNA sequencing (scRNA-seq) combined with TCR sequencing on a total of 17,635 cells (Fig. 4A and fig. S4A). We again noted that expansion elicited by the mutant YLQ peptide resulted in reduced numbers of YLQ tetramer-positive cells, consistent with our previous results (Fig. 4B). This unbiased sequencing approach led to the identification of 10 distinct clusters, showing a clear division between tetramer-negative and tetramer-positive cells (Fig. 4C and fig. S4B). For tetramer-positive (responding) cells, we identified differential clustering between WT- and mutant-stimulated cells, indicating that stimulation with mutant peptides not only leads to reduced expansion but also altered gene expression in tetramer-specific $CD8^+$ T cells (Fig. 4D). In contrast, tetramer-negative (nonresponding) WT- and mutant-stimulated cells clustered in mixed neighborhoods, further suggesting that differences can only be found in responding cells.

We next analyzed the TCR sequences of these cells. In tetramer-negative cells, we found a high diversity of TCR sequences for both WT and mutant peptide conditions (Fig. 4E and fig. S4C). In response to peptide stimulation, we found that the pool of cells consisted of a subset of clones, with five T cell clones making up more than 50% of T cells in both patients (Fig. 4E). We found the TRAV12-1 gene to be the dominant TRAV variant for both patients, as well as the two TRBV variants TRBV7-9 and TRBV2 to be prominent, which were all recently found to be part of public TCRs specific for YLQ (Fig. 4F) (*19*, *21*). We further asked whether there are T cell clones that specifically expand in response to the mutant peptide. We found expansion of the same T cell clones upon stimulation with either WT or mutant peptide (Fig. 4E).

We next investigated gene expression signatures associated with cytotoxic activity and exhaustion (*36*). Cytotoxic gene signatures were found enriched in tetramer-positive cells (as compared with tetramer-negative cells). In line with our cytotoxicity assay results,

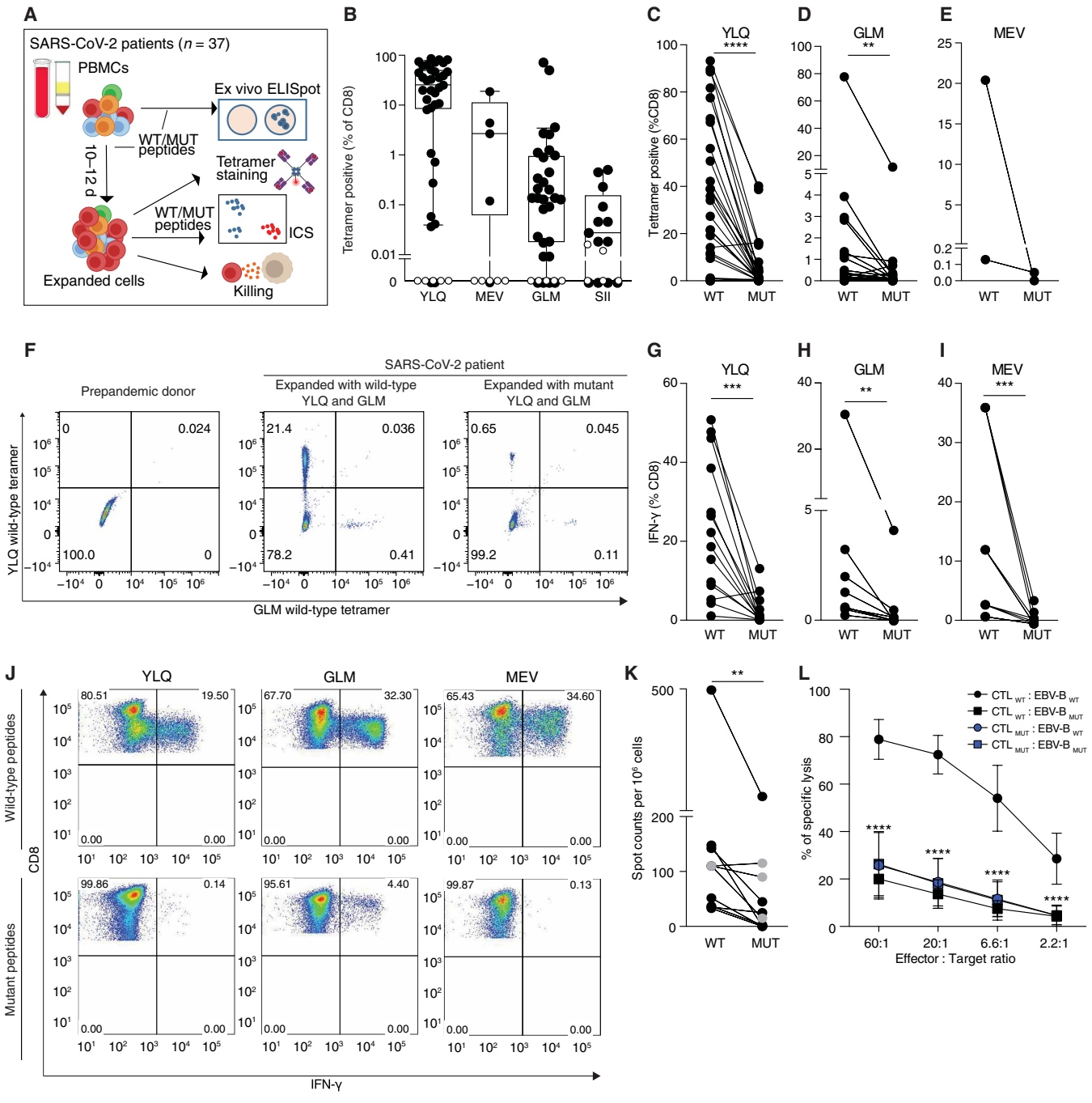

Fig. 3. SARS-CoV-2 epitope mutations are associated with decreased CTL responses. (**A**) Experimental overview. (**B**) CTL responses against WT epitopes. PBMCs were isolated from HLA-A*02:01 or HLA-B*40:01–positive SARS-CoV-2 patients (black, $n = 35$, 5, 3, or 13, respectively) or prepandemic controls with unknown HLA status (white, $n = 7$), expanded 10 to 12 days with indicated peptides, and stained with WT tetramers. Boxes show median ± 25th and 75th percentiles, and whiskers indicate 10th and 90th percentiles. (**C** to **E**) T cells expanded with mutant peptides do not give rise to WT peptide–specific CTLs. PBMCs were isolated as in (B), stimulated with WT or mutant peptides and stained with tetramers containing the WT peptide. ($n = 27$, 25, and 2 patients per epitope). (**F**) Representative FACS plots for (C) to (E). (**G** to **I**) Impact of mutations on CTL response. PBMCs expanded with WT or mutant peptides as indicated were analyzed for IFN-γ production via ICS after restimulation with WT or mutant peptide ($n = 14$, 8, and 4 patients per epitope). (**J**) Representative FACS plots for (G) to (I). (**K**) Ex vivo IFN-γ ELISpot assays from PBMCs stimulated with the YLQ peptide or the corresponding mutant ($n = 7$, PBMCs obtained 2.7 ± 0.8 weeks after symptom onset) or the MEV peptide (marked in gray) or corresponding mutant ($n = 1$, PBMCs obtained 3 weeks after symptom onset). Two or three wells were evaluated per sample and peptide. Patient ID is as indicated in table S6. (**L**) CTL killing assay. PBMCs from four patients were expanded with WT or mutant YLQ peptide and mixed with autologous EBV$^+$ B cells that were pulsed with WT or mutant YLQ peptide, and specific killing was assessed ($n = 2$ per patient). Error bars represent means ± SD. Significance is indicated as $^{**}P < 0.01$, $^{***}P < 0.001$, $^{****}P < 0.0001$, tested by Wilcoxon matched-pairs signed rank test (C), (D), (E), (G), (H), (I), and K) or two-way ANOVA followed by Dunnett's multiple comparison test (L).

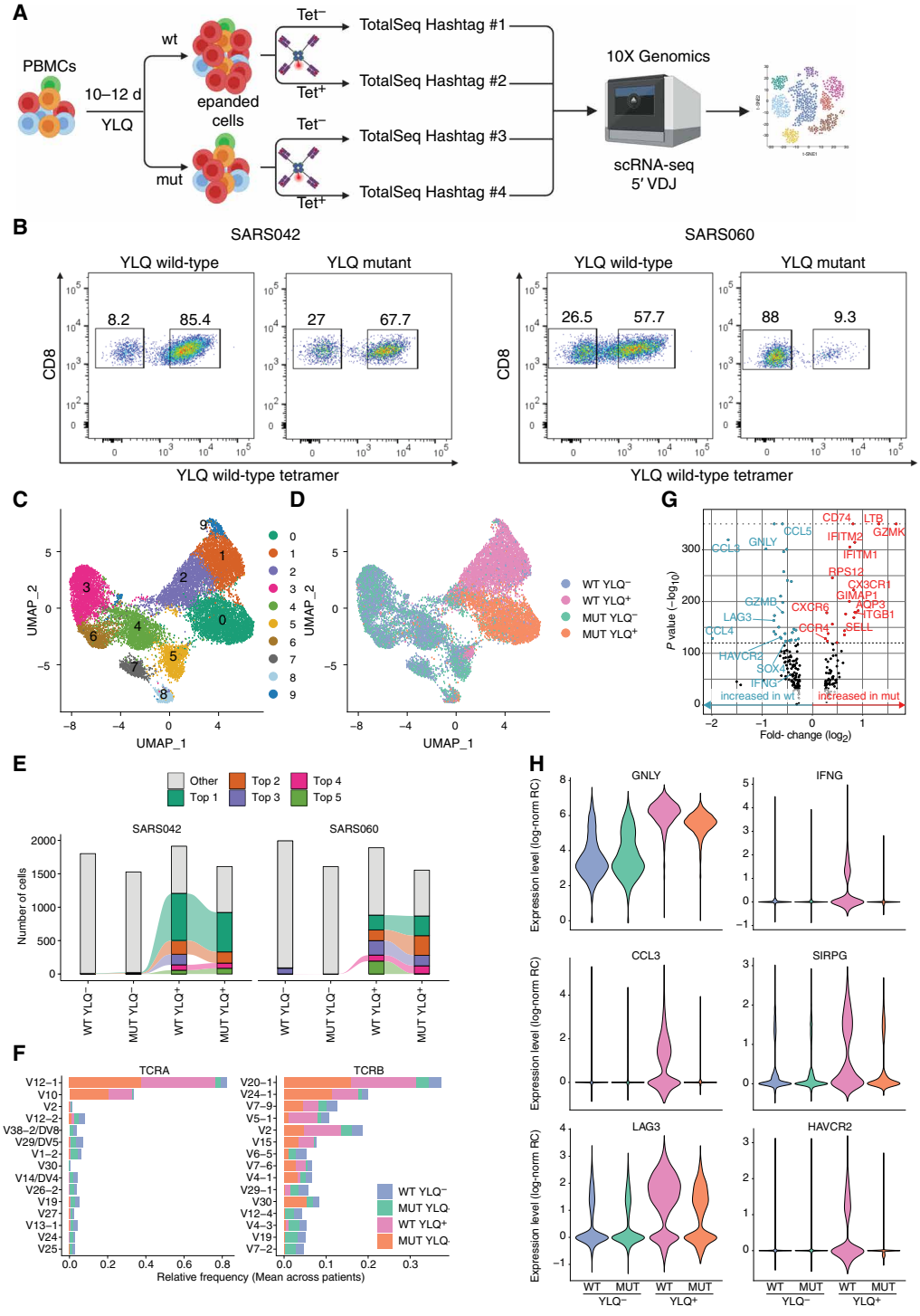

Fig. 4. Single-cell transcriptomics and TCR sequencing of CD8$^+$ T cells reveals distinct transcriptional profiles in response to mutant peptide. (**A**) Experimental setup. PBMCs were expanded for 10 to 12 days in the presence of WT or mutant YLQ peptide, sorted for YLQ tetramer–positive and tetramer-negative CD8$^+$ cells, labeled with barcoded antibodies (TotalSeq anti-human Hashtag), and subjected to scRNA-seq (figure generated with BioRender.com). (**B**) Percentages of YLQ tetramer–positive CD8$^+$ T cells in response to WT or mutant peptide expansion from the two donors analyzed. (**C** and **D**) UMAP plots displaying an embedding of single-cell transcriptomes in two-dimensional space. The cells are colored according to their clusters (C) or experimental condition (D). (**E**) Distribution of clonotypes for both patients and the indicated conditions. The top five clonotypes are colored. Connecting lines show clonotypes shared between conditions. (**F**) Top 15 TRAV and TRVB genes. (**G**) Volcano plot displaying differentially expressed genes between WT-positive and mutant-positive cells. *P* values of 0 were capped to 10^{-350} (indicated by gray dotted line). (**H**) Violin plots showing expression levels in tetramer-negative and tetramer-positive cells expanded with mutant or WT peptide. Expression levels given as log-normalized relative read counts. All plots in (C) to (H) show combined data from both patients.

we found up-regulated expression of cytotoxicity-associated genes, such as *GZMB*, *PRF1*, and *NKG7*, and decreased expression of genes associated with naïve T cell states, such as *IL7R* and *TCF7* (fig. S4, D and E). To further our understanding of qualitative differences, we performed differential gene expression analysis to compare WT and mutant peptide–stimulated cells (Fig. 4G). We identified lower expression levels of several cytotoxicity- and exhaustion-associated transcripts, such as *GZMB*, *GNLY*, the coinhibitory receptors *LAG3* and *HAVCR2*, the cytokines *IFNG*, *CCL3*, and *CCL4*, and the co-stimulatory gene *SIRPG* in mutant-stimulated T cells (Fig. 4, G and H, and fig. S4G). This is in line with a more profound exhaustion gene signature, which has recently been identified in SARS-CoV-2–specific $CD8^+$ T cells in cells stimulated with WT peptide (fig. S4F). This signature was linked in the literature to a higher expression of cytotoxicity-associated genes (*36*). These findings further underline qualitative differences in the response to expansion with mutant peptide and are in line with the results from the killing assay presented earlier (Fig. 3L). In contrast, we found a set of genes including *GZMK*, *LTB*, *CD74*, *SELL*, *IFITM1*, *IFITM2*, and *CX3CR1* expressed at higher levels in cells stimulated with mutant peptides (fig. S4F and H to K). Together, the scRNA-seq data indicate that stimulation with mutant peptide did not only lead to a reduced T cell response but also to altered gene expression patterns.

DISCUSSION

The presented data demonstrate that SARS-CoV-2 may evade CTL surveillance through mutations in viral epitopes, which lead to reduced peptide–MHC-I binding and quantitatively and qualitatively altered CTL responses. Deep SARS-CoV-2 genome sequencing results afford a valuable additional perspective that complements insights gained from numerous studies on SARS-CoV-2–specific T cell responses (*37*). Viruses use numerous strategies to evade $CD8^+$ T cell immune responses (*38*–*40*). The SARS-CoV-2–encoded ORF8 protein is hypothesized to down-regulate the surface expression of MHC-I molecules (*41*), and several reports linked mutations within the viral spike protein to the evasion of neutralizing antibody responses (*26*–*28*). Yet, we still lack a comprehensive understanding of the intrinsic capabilities of SARS-CoV-2 for immune evasion. Our study provides evidence that single nonsynonymous mutations in SARS-CoV-2 can subvert the immune response to $CD8^+$ T cell epitopes. Most nonsynonymous mutations found in the validated CTL escapes had not reached fixation, i.e., were present at frequencies between 0.02 and 0.42 (Fig. 1B). This could be explained by the shorter duration of infection with SARS-CoV-2 compared with HIV or HCV. It may also reflect on the degree to which HLA polymorphism affects viral spreading within human populations. The impact of single anchor residue substitutions on the response of $CD4^+$ T cells is still unclear.

Our findings do not rule out that substitutions of residues facing the cognate TCR may give rise to the emergence of CTL neoepitopes. We could show for the YLQ epitope that T cell clones that expanded in vitro in the presence of mutant peptides were identical to those expanded in response to the WT peptide, suggesting a similar if not identical structural basis underlying TCR-epitope engagement.

This study does not allow direct conclusions to be drawn concerning potential selection pressures, which shape the mutational landscape of $CD8^+$ T cell epitopes. This would invariably involve accounting for the HLA genotype of all individuals from whom SARS-CoV-2 genomes were sequenced. Moreover, how CTL escape mutations are maintained during transmission between individuals with differing HLA subtypes and how viruses carrying epitope mutations affect disease severity require further investigation.

Many CTL epitopes for SARS-COV-2 have been described (*37*). Natural CTL responses against SARS-CoV-2 were associated with broad epitope recognition of, on average, 1.6 $CD8^+$ T cell epitopes per antigen per HLA allele (*42*), which raises the question whether and how mutations in single epitopes affect virus control. This may be of particular importance for SARS-CoV-2 subunit vaccines, such as the RNA vaccines currently in use, which contain the S gene only and thus induce responses against a limited number of CD8 epitopes (*43*–*45*). In summary, our results highlight the capacity of SARS-CoV-2 to evade adaptive immune responses through sporadically emerging mutations in MHC-I epitopes.

MATERIALS AND METHODS

Study design

The objective of this study was to investigate mutations in SARS-CoV-2 for their potential to evade $CD8^+$ T cell responses. For this study, we performed deep sequencing on virus samples from Austria. To characterize identified mutants, we performed in vitro MHC-I binding assays. Further, we performed functional assays on PBMCs isolated from patients with COVID-19. PBMCs were only analyzed from patients who were positive for HLA-A*02:01 or HLA-B*40:01. This study was performed in accordance with the recommendations of the Declaration of Helsinki. The protocols were approved by the Ethics Committee of the Medical University of Vienna, Austria (2283/2019 and 1339/2017), and written informed consent was obtained from all patients.

Virus sample collection and processing

Virus samples were obtained from the Medical University of Vienna Institute of Virology, Medical University of Innsbruck Institute of Virology, Medical University of Innsbruck Department of Internal Medicine II and Division of Hygiene and Medical Microbiology, Central Institute for Medical-Chemical Laboratory Diagnostics Innsbruck, Klinikum Wels-Grieskirchen, and the Austrian Agency for Health and Food Safety. Sample types included oropharyngeal swabs, nasopharyngeal swabs, tracheal secretion, bronchial secretion, serum, and plasma. RNA was extracted using the following commercially available kits following the manufacturer's instructions: easyMag (bioMérieux), MagMAX (Thermo Fisher Scientific), MagNA Pure LC 2.0 (Roche), AltoStar Purification Kit 1.5 (Altona-Diagnostics), MagNA Pure Compact (Roche), and QIAsymphony (Qiagen). Viral RNA was reverse-transcribed with Superscript IV Reverse Transcriptase (Thermo Fisher Scientific), and viral sequences were amplified with modified primer pools (*46*). Polymerase chain reactions (PCRs) were pooled and processed for high-throughput sequencing.

PBMC sample collection and processing

Whole blood samples from hospitalized SARS-CoV-2–infected patients were collected at the Department of Medicine 4, Clinic Favoriten. Samples from the same individuals were collected at 2- to 7-day time intervals to obtain sufficient blood volumes for different T cell analyses. Samples from healthy blood donors that were never exposed to SARS-CoV-2 were collected before the SARS-CoV-2 pandemic (June to November 2019). PBMCs were isolated by density gradient

centrifugation and stored in liquid nitrogen until further use. HLA typing of PBMCs was carried out by next-generation sequencing, as described previously (*47*).

Virus sequencing, data processing, and analysis

AMPure XP beads (Beckman Coulter) at a 1:1 ratio were used for amplicon cleanup. Amplicon concentrations and size distribution were assessed with the Qubit Fluorometric Quantitation system (Life Technologies) and the 2100 Bioanalyzer system (Agilent), respectively. After normalization of amplicon concentrations, sequencing libraries were generated with the NEBNext Ultra II DNA Library Prep Kit for Illumina (New England Biolabs) according to the manufacturer's instructions. Library concentrations and size distribution were again assessed as indicated previously and pooled at equimolar ratios for sequencing. Sequencing was carried out on the NovaSeq 6000 platform (Illumina) on an SP flow cell with a read length of 2 × 250 base pair (bp) in paired-end mode.

After demultiplexing, FASTQ files were quality-controlled using FASTQC (v. 0.11.8) (*48*). Adapter sequences were trimmed with BBDUK from the BBTools suite (http://jgi.doe.gov/data-and-tools/bbtools). Overlaps of paired reads were corrected with the BBMERGE from BBTools. Read pairs were mapped on the combined GRCh38 and SARS-CoV-2 genome (RefSeq: NC_045512.2) using BWA-MEM with a minimal seed length of 17 (v 0.7.17) (*49*). Only reads uniquely mapping to the SARS-CoV-2 genome were retained. Primer sequences were masked with iVar (*50*). The consensus FASTA file was generated from the binary alignment map (BAM) file using Samtools (v 1.9) (*51*), mpileup, Bcftools (v 1.9) (*51*), and SEQTK (https://github.com/lh3/seqtk). The read alignment file was realigned with the Viterbi method from LoFreq (v 2.1.2) for low-frequency variant calling (*52*). InDel qualities were added, and low-frequency variants were called with LoFreq. Variants were filtered with LoFreq and Bcftools (v 1.9) (*53*). We only considered variants with a minimum coverage of 75 reads, and a minimum phred value of 90 and removed indels (insertions and deletions) followed by 4 or more identical nucleotides [homopolymers of length > 3, homopolymer length to the right of the reported indel position (HRUN) > 4] on the 3' side. On the basis of the control experiments described earlier, all analyses were performed on variants with a minimum alternative frequency of 0.02 (*54*). Variants were annotated with SnpEff (v 4.3) (*55*) and SnpSift (v 4.3) (*56*).

The output of LoFreq was filtered for nonsynonymous variants with a frequency cutoff of 0.02. The resulting mutations were then filtered for positions in reported $CD8^+$ T cell epitopes. Data manipulation and plotting were carried out in R, with the packages dplyr, tidyr, ggplot2, and heatmap2.

Identification of epitope mutations in SARS-CoV-2 genomes

Mutations in epitope regions were identified in all available protein alignment files for the SARS-CoV-2 proteins nonstructural protein 3 (NSP3, n = 164,819), NSP6 (n = 164,806), M (n = 164,846), spike (S, n = 165,249), N (n = 164,876), and E (n = 164,847) retrieved on 30 October 2020 from the GISAID database (*31*). Protein alignment files were first filtered for protein sequences that have less than 5% unknown amino acid positions. Epitope regions were then extracted from the alignment files and misaligned entries (>4 misaligned positions in epitope region), and protein sequences with more than four unknown positions in epitope regions were removed. Mutations in epitope regions were identified on the basis of sequence comparison with the reference sequence "Wuhan-Hu-1" (GenBank: MN908947.3) (*57*).

MHC-I binding predictions

To predict the binding strength of WT and mutant peptides, NetMHCpan 4.1 was used (*30*). Briefly, WT and mutant peptide sequences were interrogated for binding to HLA-A*02:01, HLA-A*02:06, and HLA-B*40:01 with the standard settings (strong binder % rank 0.5, weak binder % rank 2). The % ranks of WT and mutant epitopes were then compared and plotted along the heatmap of variant frequencies.

Peptides

Peptides were purchased from JPT Peptide Technologies GmbH or synthesized in-house, as indicated in table S2. Peptides were produced in-house by solid-phase synthesis with the 9-fluorenylmethoxy carbonyl method (CEM-Liberty and Applied Biosystems) on polyethylene glycol-polystyrene (PEG-PS) preloaded resins (Merck, Darmstadt, Germany) as previously described (*58*, *59*) with the following alterations. After synthesis, the peptides were washed with 50 ml of dichloromethane (Roth), cleaved from the resins using 28.5 ml of trifluoroacetic acid (Roth), 0.75 ml of silane (Sigma-Aldrich, St. Louis, MO, USA), and 0.575 ml of H_2O for 2.5 hours at room temperature and precipitated into prechilled *tert*-butylmethylether (Merck). The peptides were purified by reversed-phase high-performance liquid chromatography in a 10 to 70% acetonitrile gradient using a Jupiter 4 μm Proteo 90 Å LC column (Phenomenex) and an UltiMate 3000 Pump (Dionex) to a purity >90%. Their identities and molecular weights were verified by mass spectrometry (Microflex MALDI-TOF, Bruker).

Synthesis of HLA/peptide complexes.

cDNA encoding the extracellular domains of HLA-A*02:01 (UniProt: P01892), HLA-B*40:01 (UniProt: P01889), and beta-2-microglobulin (β2m; UniProt: P61769) were cloned without the leader sequence into pET-28b (HLA-A*02:01 and HLA-B*40:01) and pHN1 (β2m) for recombinant protein expression as inclusion bodies in *Escherichia coli*. pET-28b was modified to encode a C-terminal 12× poly histidine tag (HIS_{12}) or AviTag. Single colonies of *E. coli* (BL21) transformed with individual vectors were grown in 8 l Luria-Bertani (LB) medium at 37°C to an OD_{600} (optical density at 600 nm) of 0.5. Protein expression was induced by addition of isopropyl β-D-thiogalactoside (Sigma-Aldrich) to a final concentration of 1 μM. Cells were harvested after 4 hours of induction. Inclusion bodies containing HLA and β2m protein were isolated, fully denatured, and refolded in vitro in the presence of UVCP, GILGFVFJL for HLA-A*02:01, TEADVQJWL for HLA-B*40:01, and J = 3-amino-3-(2-nitro) phenyl-propionic acid) to produce HLA/UVCP protein (UVCP peptides: GILGFVFJL for HLA-A*02:01, TEADVQJWL for HLA-B*40:01, and J = 3-amino-3-(2-nitro)phenyl-propionic acid) (*32*, *60*, *61*). The refolding reaction (500 ml) was dialyzed three times against 10 liters of phosphate-buffered saline (PBS). Dialyzed HLA/UVCP HIS_{12} tag proteins were purified by nickel-nitrilotriacetic acid (Ni^{2+}-NTA) agarose chromatography (HisTrap excel, GE Healthcare) followed by size exclusion chromatography (SEC) (Superdex 200 10/300 GL, GE Healthcare). Dialyzed HLA/UVCP AviTag proteins were concentrated to 2 ml using spin concentrators and purified by SEC. Purified HLA/UVCP AviTag proteins were biotinylated using biotin protein ligase BirA as described (*62*) and further purified by SEC. The purity and integrity of all proteins were confirmed via SDS–polyacrylamide gel electrophoresis followed by silver staining.

UV-mediated peptide exchange, DSF, and tetramer synthesis

For peptide exchange, peptides were added to HLA/UVCP at an HLA/UVCP:peptide molar ratio of 1:20 (at a final concentration of 1.5 and 30 μM, respectively). For efficient cleavage, the reaction mix was placed within 5 cm from the CAMAG UV Lamp 4 (Camag) and exposed to 366-nm UV light for 2 hours at 4°C followed by 16 hours of incubation at 4°C.

For DSF, SYPRO Orange Protein Gel Stain (5000× stock solution, Thermo Fisher Scientific) was diluted at 4°C into the solution containing UV-treated HLA/peptide HIS_{12} mixtures (see above) at a final concentration of 15× SYPRO Orange Protein Gel Stain. The reaction mix was immediately transferred to prechilled PCR tubes and placed on a CFX 96 Real-Time PCR system (Bio-Rad), which had been precooled to 4°C. Samples were heated at a rate of 0.4°C/20 s, and relative fluorescence units (rfu) were measured every 20 s in the fluorescence resonance energy transfer channel. Readings were plotted as negative derivative of fluorescence change versus temperature -d(RFU)/dT. For tetramer synthesis, fluorescence-labeled streptavidin was added to UV-exchanged HLA/peptide AviTag protein solution in 10 steps as published (*63*).

Flow cytometry assays after 10 to 12 days in vitro stimulation

For in vitro expansion, cryopreserved PBMCs were thawed in prewarmed RPMI-1640 medium (R0883, Sigma-Aldrich) containing 10% fetal bovine serum (FBS 12-A, Capricorn), 10 mM Hepes (Sigma-Aldrich), 2 mM GlutaMAX (Gibco), penicillin-streptomycin (50 IU/ml; Sigma-Aldrich), and 50 IU interleukin-2 (IL-2; Peprotech) at a concentration of 1×10^6 cells/ml. PBMCs were pulsed with peptides (1 μg/ml) and cultured for 10 to 12 days, adding 100 IU of IL-2 on day 5. In vitro expanded cells were analyzed by ICS and cell surface marker staining. PBMCs were incubated with peptides (2 μg/ml) and anti-CD28/49d antibodies (1 μg/ml; L293 and L25, Becton Dickinson) or with CD28/49d antibodies alone (negative control) for 6 hours. After 2 hours, brefeldin A (0.01 μg/ml; Sigma-Aldrich) was added. Staining was performed using allophycocyanin-H7 (APC-H7) anti-human CD3 (SK7, Becton Dickinson), Pacific Blue anti-human CD4 (RPA-T4, Becton Dickinson), phycoerythrin (PE) anti-human CD8 (HIT8a, Becton Dickinson), fluorescein isothiocyanate (FITC) anti-human IFN-γ monoclonal antibodies (25723.11, Becton Dickinson), and Fix/Perm kit (Invitrogen). Viable cells were determined using live/dead cell viability assay kit (Invitrogen). Tetramer staining (10 μg/ml) was performed for 60 min at 4°C followed by staining with anti-CD8α antibody (10 μg/ml; OKT8, Invitrogen) for 30 min at 4°C.

Flow-cytometric analyses were carried out on Cytek Aurora (Cytek Biosciences) or fluorescence-activated cell sorting (FACS) Canto II (Becton Dickinson) instruments and evaluated using FlowJo software v. 7.2.5 (Tree Star). The gate for detection of IFN-γ in peptide-stimulated cell samples was set in the samples with costimulation only.

IFN-γ ELISpot assay

For ex vivo ELISpot assays, PBMCs were thawed and depleted of $CD4^+$ cells using magnetic microbeads coupled to anti-CD4 antibody and LD columns according to the manufacturer's instructions (Miltenyi Biotec). A total of 1 to 2×10^5 CD4-depleted cells per well were incubated with single peptides (2 μg/ml), AIM-V medium (negative control), or phytohemagglutinin (0.5 μg/ml, positive control; L4144, Sigma-Aldrich) in 96-well plates coated with 1.5 μg of anti–IFN-γ (1-D1K, Mabtech). After 45 hours of incubation, spots were developed with 0.1 μg of biotin-conjugated anti–IFN-γ (7-B6-1, Mabtech), streptavidin-coupled alkaline phosphatase (1:1000; Mabtech), and 5-bromo-4-chloro-3-indolyl phosphate/nitro blue tetrazolium (Sigma-Aldrich). Spots were counted in two to three wells per sample using a Bio-Sys Bioreader 5000 Pro-S/BR177 and Bioreader software generation 10. T cell responses were considered positive when mean spot counts were at least threefold higher than the mean spot counts of three unstimulated wells.

Generation of autologous EBV-transformed lymphoblastoid B cell lines

PBMCs were isolated from heparinized blood of four COVID-19 convalescent patients (SARS048, SARS047, SARS044, and SARS050) by standard Ficoll density gradient centrifugation using Lymphoprep (Technoclone). EBV-transformed lymphoblastoid B cell lines (EBV^+ B cells) were generated by supplementing PBMCs with infectious marmoset P95-8 supernatant (American Type Culture Collection) plus cyclosporin A (200 ng/ml; Sandimmune) in the presence of ODN2006 (1 μg/ml; InvivoGen) at 37°C in 5% CO_2. After 10 days of incubation, cells were replated 1:2 in fresh medium and further cultured in RPMI 1640 medium supplemented with 10% fetal calf serum, 2 mM L-glutamine, and gentamicin sulfate (100 μg/ml).

Cellular cytotoxicity assay

The cytolytic activity of CTLs was tested in standard ^{51}Cr-release assays. Autologous EBV^+ B cell cells (2×10^6/2 ml, 24-well) were pulsed with YLQ WT (YLQPRTFLL) or mutant peptide (YFQPRTFLL) or a negative control peptide (GVIMMFLSLGVGA, a nonimmunogenic yellow fever virus peptide), respectively, at a concentration of 1 μg/ml overnight. The next day, cells were harvested, resuspended in 100-μl medium, and labeled with 150 μCi of $Na^{51}CrO^4$ (PerkinElmer) at 37°C for 3 hours. After four washes, autologous EBV^+ B cells were added to round-bottom 96-well plates that contained titrated numbers of WT or mutant YLQ peptide–specific PBMCs, generated as described under "Flow cytometry assays following 10-12 days in vitro stimulation" (in duplicates). Subsequently, plates were centrifuged at 200*g* for 5 min. After 5 hours of incubation at 37°C, the supernatants were collected, and the radioactivity was determined in a γ-counter (Packard). The percentage of specific release was determined as follows: [CTL-induced release (cpm) − spontaneous release (cpm)]/[maximum release (cpm) − spontaneous release (cpm)] × 100.

Tetramer sorting, hashtag labeling, and scRNA-seq

PBMCs were harvested after 10 to 12 days of in vitro expansion (as described under "Flow cytometry assays following 10-12d in vitro stimulation") with either YLQ WT (YLQPRTFLL) or mutant peptide (YFQPRTFLL) and counted using TruCount tubes (Becton Dickinson) on a FACS Fortessa (Becton Dickinson). Cells were centrifuged at 400*g* for 5 min at 4°C and washed in ice-cold FACS buffer [Dulbecco's PBS (DPBS); Gibco] containing 1% Octaplas LG, blood group AB (Octapharma). All staining and washing steps were performed on ice. After centrifugation, the cell pellet was resuspended in 50-μl FACS buffer and stained with HLA-A*02:01 YLQ WT (YLQPRTFLL) tetramer in PE at 10 μg/ml for 20 min. Cells were washed with ice-cold FACS buffer followed by staining with FITC anti-human CD8 (SK1, Becton Dickinson) for 20 min. Cells were washed with ice-cold FACS buffer and resuspended in 200-μl FACS buffer, and dead cells were counterstained with 4′,6-diamidin-2-phenylindol

(2 μg/ml; Sigma-Aldrich). Cell sorting was performed on a FACS Aria II Cell Sorter (Becton Dickinson). For each patient, tetramer-positive and tetramer-negative cells of both WT peptide–expanded and mutant peptide–expanded cultures were sorted into 50-μl sorting buffer (DPBS; Gibco) with 0.08% bovine serum albumin (Sigma-Aldrich). Cells were centrifuged, and the supernatant was carefully discarded, leaving 50 μl behind. To this residual of 50 μl, 1 μl (0.5 μg) of TotalSeq-C0251 anti-human Hashtag Antibody 1 to 4, respectively, (394661, 394663, 394665, and 394667, all from BioLegend) was added and incubated for 20 min on ice. Cells were washed in 1-ml ice-cold sorting buffer, centrifuged, and taken up in 1-ml sorting buffer. Cells were counted again using TruCount tubes.

For each patient, volumes corresponding to 22,000 cells of each condition were pooled and centrifuged again. The cell pellet was resuspended in 80-μl sorting buffer and stored on ice until further preparation for sequencing.

scRNA-seq was performed on the live samples using the 10x Genomics Chromium Single-Cell Controller with the Chromium Single Cell 5′ v1.1 kit following the manufacturer's instructions. After cDNA amplification, TCR enrichment and enrichment of feature barcoding sequences from the hashtag antibodies were performed according to instructions by 10X Genomics manufacturer's guidelines for variable diversity joining (VDJ) and feature barcoding enrichment. After quality control, libraries were sequenced on the Illumina NovaSeq sequencing platform using the SP flow cell in 2 × 150 bp paired-end mode at the Biomedical Sequencing Facility (BSF) of the CeMM Research Center for Molecular Medicine of the Austrian Academy of Science.

Primary analysis was done using the CellRanger v5.0.1 software (10X Genomics). Alignment to the human reference transcriptome (refdata-gex-GRCh38-2020-A for gene expression and vdj_GRCh38_alts_ensembl-5.0.0 for VDJ analysis) was performed by the BSF. Hashtag Oligo identification was performed with the CITE-seq software (*64*), and demultiplexing was done with custom Python scripts by the BSF. We used the R statistics software to perform all further analysis using the Seurat package version 3.9.9.9038 (*65*). Briefly, CellRanger outputs from both patients were jointly loaded into R to perform quality control [removing cells with less than 1000 genes, mitochondrial content more than 10%, and all cells without (negatives) or with two conflicting hashtag labels (doublets)]. Preliminary clustering revealed two outlier clusters of cells shared across all conditions with higher number of counts (fig. S5), which dominated the variance and were removed from downstream analysis. Patient-dependent batch effects were then removed by integration with Seurat's FindIntegrationAnchors and Integrate data (nfeatures = 2000, dims = 1:30). The dataset was then normalized (function NormalizeData, ScaleData) to generate corrected, log-transformed relative cell counts. Integrated data were used for low-dimensional projection using Uniform Manifold Approximation and Projection (UMAP) (*66*) based on the top 10 principal components and for clustering cells (resolution = 0.6). Differential gene expression analysis was performed using the FindMarkers function (method: MAST). The adjusted *P* values returned by FindMarkers were further subjected to Bonferroni correction for the two tests applied (YLQ^+ versus YLQ^- and WT YLQ^+ versus MUT YLQ^+). For plotting, *P* values smaller than 10^{-350} were capped to 10^{-350}. The results of the differential expression analysis on raw counts (|log2 fold change| > 0.25) are reported in table S7. Gene signatures for cytotoxic, viral, unhelped, IFN-γ, and exhaustion responses were obtained from Kusnadi *et al.* (*36*), and enrichment was evaluated using R package AUCell (*67*).

For T cell clonotype analysis, the results from CellRanger were loaded into R and processed using the scRepertoire package and custom code. Clonotype identity was determined by the amino acid sequence of the assembled receptor sequences, and we focused our analysis on the five most frequent clonotypes for each of the two individuals (table S8).

Statistical analysis

Statistical analysis of differences between the WT and mutant $CD8^+$ T cell responses for ELISpot and ICS was done with Wilcoxon matched-pairs signed rank test. For comparison of >1 mutant responses, a Generalized Equation Estimations model with peptide (fixed factor) and patient (random factor) was used. For analysis of CTL killing assays, two-way analysis of variance (ANOVA) followed by Dunnett's multiple comparison test was used. Differential gene expression analysis was performed using the FindMarkers function (method: MAST). The adjusted *P* values returned by FindMarkers were further subjected to Bonferroni correction for the two tests applied (YLQ^+ versus YLQ^- and WT YLQ^+ versus MUT YLQ^+).

SUPPLEMENTARY MATERIALS

immunology.sciencemag.org/cgi/content/full/6/57/eabg6461/DC1
Figs. S1 to S5
Tables S1 to S11
Reproducibility Checklist

View/request a protocol for this paper from *Bio-protocol*.

REFERENCES AND NOTES

1. X. Zhang, Y. Tan, Y. Ling, G. Lu, F. Liu, Z. Yi, X. Jia, M. Wu, B. Shi, S. Xu, J. Chen, W. Wang, B. Chen, L. Jiang, S. Yu, J. Lu, J. Wang, M. Xu, Z. Yuan, Q. Zhang, X. Zhang, G. Zhao, S. Wang, S. Chen, H. Lu, Viral and host factors related to the clinical outcome of COVID-19. *Nature* **583**, 437–440 (2020).
2. N. Vabret, G. J. Britton, C. Gruber, S. Hegde, J. Kim, M. Kuksin, R. Levantovsky, L. Malle, A. Moreira, M. D. Park, L. Pia, E. Risson, M. Saffern, B. Salomé, M. Esai Selvan, M. P. Spindler, J. Tan, V. van der Heide, J. K. Gregory, K. Alexandropoulos, N. Bhardwaj, B. D. Brown, B. Greenbaum, Z. H. Gümüş, D. Homann, A. Horowitz, A. O. Kamphorst, M. A. Curotto de Lafaille, S. Mehandru, M. Merad, R. M. Samstein, M. Agrawal, M. Aleynick, M. Belabed, M. Brown, M. Casanova-Acebes, J. Catalan, M. Centa, A. Charap, A. Chan, S. T. Chen, J. Chung, C. C. Bozkus, E. Cody, F. Cossarini, E. Dalla, N. Fernandez, J. Grout, D. F. Ruan, P. Hamon, E. Humblin, D. Jha, J. Kodysh, A. Leader, M. Lin, K. Lindblad, D. Lozano-Ojalvo, G. Lubitz, A. Magen, Z. Mahmood, G. Martinez-Delgado, J. Mateus-Tique, E. Meritt, C. Moon, J. Noel, T. O'Donnell, M. Ota, T. Plitt, V. Pothula, J. Redes, I. Reyes Torres, M. Roberto, A. R. Sanchez-Paulete, J. Shang, A. S. Schanoski, M. Suprun, M. Tran, N. Vaninov, C. M. Wilk, J. Aguirre-Ghiso, D. Bogunovic, J. Cho, J. Faith, E. Grasset, P. Heeger, E. Kenigsberg, F. Krammer, U. Laserson, Immunology of COVID-19: Current state of the science. *Immunity* **52**, 910–941 (2020).
3. D. Mathew, J. R. Giles, A. E. Baxter, D. A. Oldridge, A. R. Greenplate, J. E. Wu, C. Alanio, L. Kuri-Cervantes, M. Betina Pampena, K. D'Andrea, S. Manne, Z. Chen, Y. J. Huang, J. P. Reilly, A. R. Weisman, C. A. G. Ittner, O. Kuthuru, J. Dougherty, K. Nzingha, N. Han, J. Kim, A. Pattekar, E. C. Goodwin, E. M. Anderson, M. E. Weirick, S. Gouma, C. P. Arevalo, M. J. Bolton, F. Chen, S. F. Lacey, H. Ramage, S. Cherry, S. E. Hensley, S. A. Apostolidis, A. C. Huang, L. A. Vella; UPenn COVID Processing Unit, M. R. Betts, N. J. Meyer, E. John Wherry, Deep immune profiling of COVID-19 patients reveals distinct immunotypes with therapeutic implications. *Science* **369**, eabc8511 (2020).
4. N. Le Bert, A. T. Tan, K. Kunasegaran, C. Y. L. Tham, M. Hafezi, A. Chia, M. H. Y. Chng, M. Lin, N. Tan, M. Linster, W. N. Chia, M. I.-C. Chen, L.-F. Wang, E. E. Ooi, S. Kalimuddin, P. A. Tambyah, J. G.-H. Low, Y.-J. Tan, A. Bertoletti, SARS-CoV-2-specific T cell immunity in cases of COVID-19 and SARS, and uninfected controls. *Nature* **584**, 457–462 (2020).
5. K. McMahan, J. Yu, N. B. Mercado, C. Loos, L. H. Tostanoski, A. Chandrashekar, J. Liu, L. Peter, C. Atyeo, A. Zhu, E. A. Bondzie, G. Dagotto, M. S. Gebre, C. Jacob-Dolan, Z. Li, F. Nampanya, S. Patel, L. Pessaint, A. Van Ry, K. Blade, J. Yalley-Ogunro, M. Cabus, R. Brown, A. Cook, E. Teow, H. Andersen, M. G. Lewis, D. A. Lauffenburger, G. Alter, D. H. Barouch, Correlates of protection against SARS-CoV-2 in rhesus macaques. *Nature* **590**, 630–634 (2021).
6. P. J. Goulder, D. I. Watkins, Impact of MHC class I diversity on immune control of immunodeficiency virus replication. *Nat. Rev. Immunol.* **8**, 619–630 (2008).
7. J. E. Schmitz, M. J. Kuroda, S. Santra, V. G. Sasseville, M. A. Simon, M. A. Lifton, P. Racz, K. Tenner-Racz, M. Dalesandro, B. J. Scallon, J. Ghrayeb, M. A. Forman, D. C. Montefiori,

E. P. Rieber, N. L. Letvin, K. A. Reimann, Control of viremia in simian immunodeficiency virus infection by $CD8^+$ lymphocytes. *Science* **283**, 857–860 (1999).
8. R. Thimme, S. Wieland, C. Steiger, J. Ghrayeb, K. A. Reimann, R. H. Purcell, F. V. Chisari, $CD8^+$ T cells mediate viral clearance and disease pathogenesis during acute hepatitis B virus infection. *J. Virol.* **77**, 68–76 (2003).
9. K. Falk, O. Rötzschke, S. Stevanović, G. Jung, H.-G. Rammensee, Allele-specific motifs revealed by sequencing of self-peptides eluted from MHC molecules. *Nature* **351**, 290–296 (1991).
10. H.-G. Rammensee, K. Falk, O. Rötzschke, MHC molecules as peptide receptors. *Curr. Opin. Immunol.* **5**, 35–44 (1993).
11. J. Braun, L. Loyal, M. Frentsch, D. Wendisch, P. Georg, F. Kurth, S. Hippenstiel, M. Dingeldey, B. Kruse, F. Fauchere, E. Baysal, M. Mangold, L. Henze, R. Lauster, M. A. Mall, K. Beyer, J. Röhmel, S. Voigt, J. Schmitz, S. Miltenyi, I. Demuth, M. A. Müller, A. Hocke, M. Witzenrath, N. Suttorp, F. Kern, U. Reimer, H. Wenschuh, C. Drosten, V. M. Corman, C. Giesecke-Thiel, L. E. Sander, A. Thiel, SARS-CoV-2-reactive T cells in healthy donors and patients with COVID-19. *Nature* **587**, 270–274 (2020).
12. T. Sekine, A. Perez-Potti, O. Rivera-Ballesteros, K. Strålin, J.-B. Gorin, A. Olsson, S. Llewellyn-Lacey, H. Kamal, G. Bogdanovic, S. Muschiol, D. J. Wullimann, T. Kammann, J. Emgård, T. Parrot, E. Folkesson; Karolinska COVID- Study Group, O. Rooyackers, L. I. Eriksson, J.-I. Henter, A. Sönnerborg, T. Allander, J. Albert, M. Nielsen, J. Klingström, S. Gredmark-Russ, N. K. Björkström, J. K. Sandberg, D. A. Price, H.-G. Ljunggren, S. Aleman, M. Buggert, Robust T cell immunity in convalescent individuals with asymptomatic or mild COVID-19. *Cell* **183**, 158–168.e14 (2020).
13. A. Grifoni, D. Weiskopf, S. I. Ramirez, J. Mateus, J. M. Dan, C. R. Moderbacher, S. A. Rawlings, A. Sutherland, L. Premkumar, R. S. Jadi, D. Marrama, A. M. de Silva, A. Frazier, A. F. Carlin, J. A. Greenbaum, B. Peters, F. Krammer, D. M. Smith, S. Crotty, A. Sette, Targets of T cell responses to SARS-CoV-2 coronavirus in humans with COVID-19 disease and unexposed individuals. *Cell* **181**, 1489–1501.e15 (2020).
14. I. Schulien, J. Kemming, V. Oberhardt, K. Wild, L. M. Seidel, S. Killmer, Sagar, F. Daul, M. S. Lago, A. Decker, H. Luxenburger, B. Binder, D. Bettinger, O. Sogukpinar, S. Rieg, M. Panning, D. Huzly, M. Schwemmle, G. Kochs, C. F. Waller, A. Nieters, D. Duerschmied, F. Emmerich, H. E. Mei, A. R. Schulz, S. Llewellyn-Lacey, D. A. Price, T. Boettler, B. Bengsch, R. Thimme, M. Hofmann, C. Neumann-Haefelin, Characterization of pre-existing and induced SARS-CoV-2-specific $CD8^+$ T cells. *Nat. Med.* **27**, 78–85 (2021).
15. J. M. Dan, J. Mateus, Y. Kato, K. M. Hastie, E. D. Yu, C. E. Faliti, A. Grifoni, S. I. Ramirez, S. Haupt, A. Frazier, C. Nakao, V. Rayaprolu, S. A. Rawlings, B. Peters, F. Krammer, V. Simon, E. O. Saphire, D. M. Smith, D. Weiskopf, A. Sette, S. Crotty, Immunological memory to SARS-CoV-2 assessed for up to eight months after infection. *Science* **371**, eabf4063 (2021).
16. A. Sette, S. Crotty, Adaptive immunity to SARS-CoV-2 and COVID-19. *Cell* **184**, 861–880 (2021).
17. A. Poran, D. Harjanto, M. Malloy, C. M. Arieta, D. A. Rothenberg, D. Lenkala, M. M. van Buuren, T. A. Addona, M. S. Rooney, L. Srinivasan, R. B. Gaynor, Sequence-based prediction of SARS-CoV-2 vaccine targets using a mass spectrometry-based bioinformatics predictor identifies immunogenic T cell epitopes. *Genome Med.* **12**, 70 (2020).
18. A. Grifoni, J. Sidney, Y. Zhang, R. H. Scheuermann, B. Peters, A. Sette, A sequence homology and bioinformatic approach can predict candidate targets for immune responses to SARS-CoV-2. *Cell Host Microbe* **27**, 671–680.e2 (2020).
19. A. S. Shomuradova, M. S. Vagida, S. A. Sheetikov, K. V. Zornikova, D. Kiryukhin, A. Titov, I. O. Peshkova, A. Khmelevskaya, D. V. Dianov, M. Malasheva, A. Shmelev, Y. Serdyuk, D. V. Bagaev, A. Pivnyuk, D. S. Shcherbinin, A. V. Maleeva, N. T. Shakirova, A. Pilunov, D. B. Malko, E. G. Khamaganova, B. Biderman, A. Ivanov, M. Shugay, G. A. Efimov, SARS-CoV-2 epitopes are recognized by a public and diverse repertoire of human T cell receptors. *Immunity* **53**, 1245–1257.e5 (2020).
20. A. Nelde, T. Bilich, J. S. Heitmann, Y. Maringer, H. R. Salih, M. Roerden, M. Lübke, J. Bauer, J. Rieth, M. Wacker, A. Peter, S. Hörber, B. Traenkle, P. D. Kaiser, U. Rothbauer, M. Becker, D. Junker, G. Krause, M. Strengert, N. Schneiderhan-Marra, M. F. Templin, T. O. Joos, D. J. Kowalewski, V. Stos-Zweifel, M. Fehr, A. Rabsteyn, V. Mirakaj, J. Karbach, E. Jäger, M. Graf, L.-C. Gruber, D. Rachfalski, B. Preuß, I. Hagelstein, M. Märklin, T. Bakchoul, C. Gouttefangeas, O. Kohlbacher, R. Klein, S. Stevanović, H.-G. Rammensee, J. S. Walz, SARS-CoV-2-derived peptides define heterologous and COVID-19-induced T cell recognition. *Nat. Immunol.* **22**, 74–85 (2021).
21. A. P. Ferretti, T. Kula, Y. Wang, D. M. V. Nguyen, A. Weinheimer, G. S. Dunlap, Q. Xu, N. Nabilsi, C. R. Perullo, A. W. Cristofaro, H. J. Whitton, A. Virbasius, K. J. Olivier Jr., L. R. Buckner, A. T. Alistar, E. D. Whitman, S. A. Bertino, S. Chattopadhyay, G. M. Beath, Unbiased screens show $CD8^+$ T cells of COVID-19 patients recognize shared epitopes in SARS-CoV-2 that largely reside outside the spike protein. *Immunity* **53**, 1095–1107.e3 (2020).
22. H. Pircher, D. Moskophidis, U. Rohrer, K. Bürki, H. Hengartner, R. M. Zinkernagel, Viral escape by selection of cytotoxic T cell-resistant virus variants in vivo. *Nature* **346**, 629–633 (1990).
23. P. J. R. Goulder, C. Brander, Y. Tang, C. Tremblay, R. A. Colbert, M. M. Addo, E. S. Rosenberg, T. Nguyen, R. Allen, A. Trocha, M. Altfeld, S. He, M. Bunce, R. Funkhouser, S. I. Pelton, S. K. Burchett, K. M. Intosh, B. T. M. Korber, B. D. Walker, Evolution and transmission of stable CTL escape mutations in HIV infection. *Nature* **412**, 334–338 (2001).
24. A. L. Cox, T. Mosbruger, Q. Mao, Z. Liu, X.-H. Wang, H.-C. Yang, J. Sidney, A. Sette, D. Pardoll, D. L. Thomas, S. C. Ray, Cellular immune selection with hepatitis C virus persistence in humans. *J. Exp. Med.* **201**, 1741–1752 (2005).
25. K. Deng, M. Pertea, A. Rongvaux, L. Wang, C. M. Durand, G. Ghiaur, J. Lai, H. L. McHugh, H. Hao, H. Zhang, J. B. Margolick, C. Gurer, A. J. Murphy, D. M. Valenzuela, G. D. Yancopoulos, S. G. Deeks, T. Strowig, P. Kumar, J. D. Siliciano, S. L. Salzberg, R. A. Flavell, L. Shan, R. F. Siliciano, Broad CTL response is required to clear latent HIV-1 due to dominance of escape mutations. *Nature* **517**, 381–385 (2015).
26. K. R. Mccarthy, L. J. Rennick, S. Nambulli, L. R. Robinson-McCarthy, W. G. Bain, G. Haidar, W. Paul Duprex, Recurrent deletions in the SARS-CoV-2 spike glycoprotein drive antibody escape. *Science* **371**, 1139–1142 (2021).
27. A. J. Greaney, T. N. Starr, P. Gilchuk, S. J. Zost, E. Binshtein, A. N. Loes, S. K. Hilton, J. Huddleston, R. Eguia, K. H. D. Crawford, A. S. Dingens, R. S. Nargi, R. E. Sutton, N. Suryadevara, P. W. Rothlauf, Z. Liu, S. P. J. Whelan, R. H. Carnahan, J. E. Crowe Jr., J. D. Bloom, Complete mapping of mutations to the SARS-CoV-2 spike receptor-binding domain that escape antibody recognition. *Cell Host Microbe* **29**, 44–57.e9 (2021).
28. P.-A. Koenig, H. Das, H. Liu, B. M. Kümmerer, F. N. Gohr, L.-M. Jenster, L. D. J. Schiffelers, Y. M. Tesfamariam, M. Uchima, J. D. Wuerth, K. Gatterdam, N. Ruetalo, M. H. Christensen, C. I. Fandrey, S. Normann, J. M. P. Tödtmann, S. Pritzl, L. Hanke, J. Boos, M. Yuan, X. Zhu, J. L. Schmid-Burgk, H. Kato, M. Schindler, I. A. Wilson, M. Geyer, K. U. Ludwig, B. Martin Hällberg, N. C. Wu, F. I. Schmidt, Structure-guided multivalent nanobodies block SARS-CoV-2 infection and suppress mutational escape. *Science* **371**, eabe6230 (2021).
29. F. F. Gonzalez-Galarza, A. McCabe, E. J. Melo Dos Santos, J. Jones, L. Takeshita, N. D. Ortega-Rivera, G. M. Del Cid-Pavon, K. Ramsbottom, G. Ghattaoraya, A. Alfirevic, D. Middleton, A. R. Jones, Allele frequency net database (AFND) 2020 update: Gold-standard data classification, open access genotype data and new query tools. *Nucleic Acids Res.* **48**, D783–D788 (2019).
30. B. Reynisson, B. Alvarez, S. Paul, B. Peters, M. Nielsen, NetMHCpan-4.1 and NetMHCIIpan-4.0: Improved predictions of MHC antigen presentation by concurrent motif deconvolution and integration of MS MHC eluted ligand data. *Nucleic Acids Res.* **48**, W449–W454 (2020).
31. Y. Shu, J. McCauley, GISAID: Global initiative on sharing all influenza data – from vision to reality. *Eurosurveillance* **22**, 30494 (2017).
32. M. Toebes, M. Coccoris, A. Bins, B. Rodenko, R. Gomez, N. J. Nieuwkoop, W. van de Kasteele, G. F. Rimmelzwaan, J. B. A. G. Haanen, H. Ovaa, T. N. M. Schumacher, Design and use of conditional MHC class I ligands. *Nat. Med.* **12**, 246–251 (2006).
33. D. T. Blaha, S. D. Anderson, D. M. Yoakum, M. V. Hager, Y. Zha, T. F. Gajewski, D. M. Kranz, High-throughput stability screening of neoantigen/HLA complexes improves immunogenicity predictions. *Cancer Immunol. Res.* **7**, 50–61 (2019).
34. K. Gao, R. Oerlemans, M. R. Groves, Theory and applications of differential scanning fluorimetry in early-stage drug discovery. *Biophys. Rev.* **12**, 85–104 (2020).
35. F. H. Niesen, H. Berglund, M. Vedadi, The use of differential scanning fluorimetry to detect ligand interactions that promote protein stability. *Nat. Protoc.* **2**, 2212–2221 (2007).
36. A. Kusnadi, C. Ramírez-Suástegui, V. Fajardo, S. J. Chee, B. J. Meckiff, H. Simon, E. Pelosi, G. Seumois, F. Ay, P. Vijayanand, C. H. Ottensmeier, Severely ill COVID-19 patients display impaired exhaustion features in SARS-CoV-2-reactive $CD8^+$ T cells. *Sci. Immunol.* **6**, eabe4782 (2021).
37. D. M. Altmann, R. J. Boyton, SARS-CoV-2 T cell immunity: Specificity, function, durability, and role in protection. *Sci. Immunol.* **5**, eabd6160 (2020).
38. T. H. Hansen, M. Bouvier, MHC class I antigen presentation: Learning from viral evasion strategies. *Nat. Rev. Immunol.* **9**, 503–513 (2009).
39. A. Alcami, U. H. Koszinowski, Viral mechanisms of immune evasion. *Trends Microbiol.* **8**, 410–418 (2000).
40. P. J. R. Goulder, D. I. Watkins, HIV and SIV CTL escape: Implications for vaccine design. *Nat. Rev. Immunol.* **4**, 630–640 (2004).
41. Y. Zhang, Y. Chen, Y. Li, F. Huang, B. Luo, Y. Yuan, B. Xia, X. Ma, T. Yang, F. Yu, J. Liu, B. Liu, Z. Song, J. Chen, S. Yan, L. Wu, T. Pan, X. Zhang, R. Li, W. Huang, X. He, F. Xiao, J. Zhang, H. Zhang, The ORF8 Protein of SARS-CoV-2 Mediates Immune Evasion through Potently Downregulating MHC-I. *Proc. Natl. Acad. Sci. U.S.A.* **118**, e2024202118 (2021).
42. A. Tarke, J. Sidney, C. K. Kidd, J. M. Dan, S. I. Ramirez, E. D. Yu, J. Mateus, R. da Silva Antunes, E. Moore, P. Rubiro, N. Methot, E. Phillips, S. Mallal, A. Frazier, S. A. Rawlings, J. A. Greenbaum, B. Peters, D. M. Smith, S. Crotty, D. Weiskopf, A. Grifoni, A. Sette, Comprehensive analysis of T cell immunodominance and immunoprevalence of SARS-CoV-2 epitopes in COVID-19 cases. *Cell Reports Med.* **2**, 100204 (2021).
43. G. Liu, B. Carter, D. K. Gifford, Predicted cellular immunity population coverage gaps for SARS-CoV-2 subunit vaccines and their augmentation by compact peptide sets. *Cell Syst.* **12**, 102–107.e4 (2021).
44. U. Sahin, A. Muik, E. Derhovanessian, I. Vogler, L. M. Kranz, M. Vormehr, A. Baum, K. Pascal, J. Quandt, D. Maurus, S. Brachtendorf, V. Lörks, J. Sikorski, R. Hilker, D. Becker, A.-K. Eller, J. Grützner, C. Boesler, C. Rosenbaum, M.-C. Kühnle, U. Luxemburger, A. Kemmer-Brück, D. Langer, M. Bexon, S. Bolte, K. Karikó, T. Palanche, B. Fischer, A. Schultz, P.-Y. Shi, C. Fontes-Garfias, J. L. Perez, K. A. Swanson, J. Loschko, I. L. Scully, M. Cutler, W. Kalina, C. A. Kyratsous, D. Cooper, P. R. Dormitzer, K. U. Jansen, Ö. Türeci, COVID-19 vaccine BNT162b1 elicits human antibody and TH1 T cell responses. *Nature* **586**, 594–599 (2020).

45. K. S. Corbett, D. K. Edwards, S. R. Leist, O. M. Abiona, S. Boyoglu-Barnum, R. A. Gillespie, S. Himansu, A. Schäfer, C. T. Ziwawo, A. T. DiPiazza, K. H. Dinnon, S. M. Elbashir, C. A. Shaw, A. Woods, E. J. Fritch, D. R. Martinez, K. W. Bock, M. Minai, B. M. Nagata, G. B. Hutchinson, K. Wu, C. Henry, K. Bahl, D. Garcia-Dominguez, L.-Z. Ma, I. Renzi, W. P. Kong, S. D. Schmidt, L. Wang, Y. Zhang, E. Phung, L. A. Chang, R. J. Loomis, N. E. Altaras, E. Narayanan, M. Metkar, V. Presnyak, C. Liu, M. K. Louder, W. Shi, K. Leung, E. S. Yang, A. West, K. L. Gully, L. J. Stevens, N. Wang, D. Wrapp, N. A. Doria-Rose, G. Stewart-Jones, H. Bennett, G. S. Alvarado, M. C. Nason, T. J. Ruckwardt, J. S. McLellan, M. R. Denison, J. D. Chappell, I. N. Moore, K. M. Morabito, J. R. Mascola, R. S. Baric, A. Carfi, B. S. Graham, SARS-CoV-2 mRNA vaccine design enabled by prototype pathogen preparedness. *Nature* **586**, 567–571 (2020).
46. K. Itokawa, T. Sekizuka, M. Hashino, R. Tanaka, M. Kuroda, Disentangling primer interactions improves SARS-CoV-2 genome sequencing by multiplex tiling PCR. *PLOS ONE* **15**, e0239403 (2020).
47. I. Faé, S. Wenda, C. Grill, G. F. Fischer, HLA-B*44:138Q : Evidence for a confined deletion and recombination events in an otherwise unaffected HLA-haplotype. *HLA* **93**, 89–96 (2019).
48. S. Andrews, FastQC - A quality control tool for high throughput sequence data, http://bioinformatics.babraham.ac.uk/projects/fastqc/, *Babraham Bioinforma.* (2010); http://bioinformatics.babraham.ac.uk/projects/.
49. H. Li, R. Durbin, Fast and accurate short read alignment with Burrows-Wheeler transform. *Bioinformatics* **25**, 1754–1760 (2009).
50. N. D. Grubaugh, K. Gangavarapu, J. Quick, N. L. Matteson, J. G. de Jesus, B. J. Main, A. L. Tan, L. M. Paul, D. E. Brackney, S. Grewal, N. Gurfield, K. K. A. van Rompay, S. Isern, S. F. Michael, L. L. Coffey, N. J. Loman, K. G. Andersen, An amplicon-based sequencing framework for accurately measuring intrahost virus diversity using PrimalSeq and iVar. *Genome Biol.* **20**, 8 (2019).
51. H. Li, B. Handsaker, A. Wysoker, T. Fennell, J. Ruan, N. Homer, G. Marth, G. Abecasis, R. Durbin; 1000 Genome Project Data Processing Subgroup, The sequence alignment/map format and SAMtools. *Bioinformatics* **25**, 2078–2079 (2009).
52. A. Wilm, P. P. K. Aw, D. Bertrand, G. H. T. Yeo, S. H. Ong, C. H. Wong, C. C. Khor, R. Petric, M. L. Hibberd, N. Nagarajan, LoFreq: A sequence-quality aware, ultra-sensitive variant caller for uncovering cell-population heterogeneity from high-throughput sequencing datasets. *Nucleic Acids Res.* **40**, 11189–11201 (2012).
53. H. Li, A statistical framework for SNP calling, mutation discovery, association mapping and population genetical parameter estimation from sequencing data. *Bioinformatics* **27**, 2987–2993 (2011).
54. A. Popa, J.-W. Genger, M. D. Nicholson, T. Penz, D. Schmid, S. W. Aberle, B. Agerer, A. Lercher, L. Endler, H. Colaço, M. Smyth, M. Schuster, M. L. Grau, F. Martínez-Jiménez, O. Pich, W. Borena, E. Pawelka, Z. Keszei, M. Senekowitsch, J. Laine, J. H. Aberle, M. Redlberger-Fritz, M. Karolyi, A. Zoufaly, S. Maritschnik, M. Borkovec, P. Hufnagl, M. Nairz, G. Weiss, M. T. Wolfinger, D. von Laer, G. Superti-Furga, N. Lopez-Bigas, E. Puchhammer-Stöckl, F. Allerberger, F. Michor, C. Bock, A. Bergthaler, Genomic epidemiology of superspreading events in Austria reveals mutational dynamics and transmission properties of SARS-CoV-2. *Sci. Transl. Med.* **12**, eabe2555 (2020).
55. P. Cingolani, A. Platts, L. L. Wang, M. Coon, T. Nguyen, L. Wang, S. J. Land, X. Lu, D. M. Ruden, A program for annotating and predicting the effects of single nucleotide polymorphisms, SnpEff: SNPs in the genome of *Drosophila melanogaster* strain w^{1118}; iso-2; iso-3. *Fly (Austin)* **6**, 80–92 (2012).
56. P. Cingolani, V. M. Patel, M. Coon, T. Nguyen, S. J. Land, D. M. Ruden, X. Lu, Using *Drosophila melanogaster* as a model for genotoxic chemical mutational studies with a new program, SnpSift. *Front. Genet.* **3**, 35 (2012).
57. F. Wu, S. Zhao, B. Yu, Y.-M. Chen, W. Wang, Z.-G. Song, Y. Hu, Z.-W. Tao, J.-H. Tian, Y.-Y. Pei, M.-L. Yuan, Y.-L. Zhang, F.-H. Dai, Y. Liu, Q.-M. Wang, J.-J. Zheng, L. Xu, E.-C. Holmes, Y.-Z. Zhang, A new coronavirus associated with human respiratory disease in China. *Nature* **579**, 265–269 (2020).
58. K. Niespodziana, K. Stenberg-Hammar, S. Megremis, C. R. Cabauatan, K. Napora-Wijata, P. C. Vacal, D. Gallerano, C. Lupinek, D. Ebner, T. Schlederer, C. Harwanegg, C. Söderhäll, M. van Hage, G. Hedlin, N. G. Papadopoulos, R. Valenta, PreDicta chip-based high resolution diagnosis of rhinovirus-induced wheeze. *Nat. Commun.* **9**, 2382 (2018).
59. D. Gallerano, E. Wollmann, C. Lupinek, T. Schlederer, D. Ebner, C. Harwanegg, K. Niespodziana, K. Schmetterer, W. Pickl, E. Puchhammer-Stöckl, E. Sibanda, R. Valenta, HIV microarray for the mapping and characterization of HIV-specific antibody responses. *Lab Chip* **15**, 1574–1589 (2015).
60. D. N. Garboczi, D. T. Hung, D. C. Wiley, HLA-A2-peptide complexes: Refolding and crystallization of molecules expressed in Escherichia coli and complexed with single antigenic peptides. *Proc. Natl. Acad. Sci. U.S.A.* **89**, 3429–3433 (1992).
61. C. S. Clements, L. Kjer-Nielsen, W. A. MacDonald, A. G. Brooks, A. W. Purcell, J. McCluskey, J. Rossjohn, The production, purification and crystallization of a soluble heterodimeric form of a highly selected T-cell receptor in its unliganded and liganded state. *Acta Crystallogr. Sect. D Biol. Crystallogr.* **58**, 2131–2134 (2002).
62. M. Fairhead, M. Howarth, Site-specific biotinylation of purified proteins using BirA, in *Methods in Molecular Biology* (Humana Press, 2015), pp. 171–184; http://link.springer.com/10.1007/978-1-4939-2272-7_12.
63. J. D. Altman, P. A. H. Moss, P. J. R. Goulder, D. H. Barouch, M. G. McHeyzer-Williams, J. I. Bell, A. J. McMichael, M. M. Davis, Phenotypic analysis of antigen-specific T lymphocytes. *Science* **274**, 94–96 (1996).
64. M. Stoeckius, C. Hafemeister, W. Stephenson, B. Houck-Loomis, P. K. Chattopadhyay, H. Swerdlow, R. Satija, P. Smibert, Simultaneous epitope and transcriptome measurement in single cells. *Nat. Methods* **14**, 865–868 (2017).
65. T. Stuart, A. Butler, P. Hoffman, C. Hafemeister, E. Papalexi, W. M. Mauck III, Y. Hao, M. Stoeckius, P. Smibert, R. Satija, Comprehensive integration of single-cell data. *Cell* **177**, 1888–1902.e21 (2019).
66. L. McInnes, J. Healy, J. Melville, UMAP: Uniform manifold approximation and projection for dimension reduction. arXiv:1802.03426 [stat.ML], (2018), pp. 1–18.
67. S. Aibar, M. Abaigar, F. J. Campos-Laborie, J. M. Sánchez-Santos, J. M. Hernandez-Rivas, J. de Las Rivas, Identification of expression patterns in the progression of disease stages by integration of transcriptomic data. *BMC Bioinformatics* **17**, 432 (2016).

Acknowledgments: We would like to thank the Biomedical Sequencing Facility at CeMM for assistance with next-generation sequencing. We thank U. Sinzinger, A. Popovitsch, and M. Zabel for excellent technical assistance, R. Sommer for helping with UV-irradiation equipment, and J. Leitner for providing reagents used in cytotoxicity assays. We would like to thank L. Domnanovich from the FACS Core Unit at CCRI for performing the tetramer sort; we thank L. Flatz, G. Superti-Furga, M. Jäger, L. Antonio Herrera, D. Zehn, and R. Zinkernagel for valuable feedback and comments. We thank the NIH Tetramer Core Facility for providing tetramer reagents that were used in preliminary experiments. We thank S. Maurer-Stroh for providing help to generate the acknowledgment table for sequences downloaded from GISAID (table S10). **Funding:** B.A. was supported by the Austrian Science Fund (FWF) DK W1212. M.S. and A.L. were supported by DOC fellowships of the Austrian Academy of Sciences (nos. 24813, 24158, and 24955 respectively). V.G., V.M., and J.B.H. received support from the Vienna Science and Technology Fund (WWTF, LS14-031). J.H.A. was supported by the Medical-Scientific fund of the Mayor of the federal capital Vienna (grant COVID003). W.F.P. was supported by the Medical-Scientific fund of the Mayor of the federal capital Vienna (grant COVID006). C.B. and A.B. were supported by ERC Starting Grants (European Union's Horizon 2020 research and innovation program, grant agreement numbers 679146 and 677006, respectively). This project was funded in part by two grants from the Vienna Science and Technology Fund (WWTF) as part of the WWTF COVID-19 Rapid Response Funding 2020 awarded to A.B. and R.G., respectively. **Competing interests:** The authors declare that they have no competing interests. **Author Contributions:** B.A., M.K., V.G, D.M.F., V.M., M.G., A.H., L.E.S., A.L., P.G., D.T., T.P., I.F., S.W., M.T., W.F.P., R.V., W.P., R.G., M.F., J.B.H., and J.H.A. performed experiments and/or generated reagents and/or provided experimental advice. B.A., L.F.M.G., M.S., A.P., J.W.G., L.E., R.T.G., D.B., and F.H. performed bioinformatic analysis of virus derived sequences or scRNA-seq data. S.W.A., G.W., V.T., F.A., H.S., E.P.S., W.W., G.F., W.H., E.P., A.Z., and C.B. provided reagents and/or patient samples and/or critically reviewed the manuscript. B.A., M.K., V.G., J.B.H., J.H.A., and A.B. wrote and/or edited the manuscript. **Data and materials availability:** Raw BAM files were submitted for inclusion in the COVID-19 Data Portal hosted by the European Bioinformatics Institute under project numbers PRJEB39849 and PRJEB42987. Consensus virus sequences are deposited in the GISAID database. The pipeline used for calling low frequency mutations is available on GitHub (https://github.com/Bergthalerlab/SARSCoV2_Code). scRNA-seq data have been deposited at the European Genome-phenome Archive (EGA), under accession number EGAS00001005060. Processed scRNA-seq data are available via Gene Expression Omnibus (GEO) under accession number GSE166651. The R code used for the analysis for scRNA-seq data will be shared via GitHub (https://github.com/cancerbits).

Submitted 19 January 2021
Accepted 27 February 2021
Published First Release 4 March 2021
Final published 1 September 2021
10.1126/sciimmunol.abg6461

Citation: B. Agerer, M. Koblischke, V. Gudipati, L. F. Montaño-Gutierrez, M. Smyth, A. Popa, J.-W. Genger, L. Endler, D. M. Florian, V. Mühlgrabner, M. Graninger, S. W. Aberle, A.-M. Husa, L. E. Shaw, A. Lercher, P. Gattinger, R. Torralba-Gombau, D. Trapin, T. Penz, D. Barreca, I. Fae, S. Wenda, M. Traungott, G. Walder, W. F. Pickl, V. Thiel, F. Allerberger, H. Stockinger, E. Puchhammer-Stöckl, W. Weninger, G. Fischer, W. Hoepler, E. Pawelka, A. Zoufaly, R. Valenta, C. Bock, W. Paster, R. Geyeregger, M. Farlik, F. Halbritter, J. B. Huppa, J. H. Aberle, A. Bergthaler, SARS-CoV-2 mutations in MHC-I–restricted epitopes evade $CD8^+$ T cell responses. *Sci. Immunol.* **6**, eabg6461 (2021).